Inorganic and organic P retention by coprecipitation during ferrous iron oxidation

Inorganic and organic P retention by coprecipitation during ferrous iron oxidation

Veronica Santoro[a,c], Maria Martin[a], Per Persson[c], Cristina Lerda[a], Daniel Said-Pullicino[a], Giuliana Magnacca[b], Luisella Celi[a]

[a] Dept. of Agricultural, Forest and Food Sciences, University of Torino, Largo P. Braccini 2, 10095 Grugliasco, Italy

[b] Dept. of Chemistry, University of Torino, via P. Giuria 7, 10125 Torino, Italy

[c] Centre for Environmental and Climate Research & Department of Biology, Lund University, 223 62 Lund, Sweden.

Corresponding author: Veronica Santoro

e-mail: veronica.santoro@unito.it

Highlights

- Coprecipitation of inorganic P (Pi), inositol hexaphosphate (*myo*InsP6) and phosphatidylcholine (PC) during Fe(II) oxidation was evaluated
- Coprecipitation offers a much higher organic P retention than adsorption
- Fe(II) oxidative precipitation kinetics were strongly affected by Pi and *myo*InsP6, but not by PC
- Coprecipitation of Pi and *myo*InsP6 strongly influenced surface properties as a function of initial P/Fe ratio

Coprecipitation is a complex process playing a pivotal role in the fate of organic P compounds in soil

Abstract

Phosphorous (P) cycling is often closely coupled to iron (Fe), particularly following mineral weathering or in hydromorphic soils where Fe redox reactions can control the equilibrium between P retention and release. While surface adsorption of P on Fe (hydr)oxides is a well-known and widely studied process, less attention has been devoted to the understanding of P (especially organic P)

coprecipitation following Fe(II) oxidative precipitation. In this work we synthesized and followed the kinetics of a series of Fe-P systems with increasing P/Fe ratio, prepared by either surface adsorption on ferrihydrite (Fh) or oxidative coprecipitation of Fe(II) with inorganic phosphate (Pi), inositol hexaphosphate (*myo*InsP6) or phosphatidylcholine (PC). The obtained materials were characterized for P and Fe contents, specific surface area (SSA), porosity and surface charge. XRD, TEM, XPS and IR techniques were used to investigate their properties. Coprecipitation resulted in generally greater P retention with respect to adsorption, especially at the highest initial P/Fe ratio. Inorganic phosphate caused interference and poisoning of the crystallization process, slowing down Fe(II) oxidation and precipitation rates at low P/Fe ratios, with the formation of nanometric particles and phosphate concentrated on their surface. With increasing P loadings, more aggregated particles with a lower SSA and greater porosity were obtained. Aside from precipitation, the retention mechanisms involved also adsorption and/or inclusion of Pi within the particles. *myo*InsP6 instead accelerated the precipitation of Fe, leading to coprecipitates bearing the organic P compound within the structure, retained by precipitation and adsorption mechanisms. Conversely, PC did not influence the rate of Fe(II) oxidation and precipitation, due to its hydrophobic features and irrespective of the P/Fe ratio. The prevailing mechanism involved in the retention of PC during coprecipitation was physical retention on the surface, leading to a drastic decrease of SSA and pore volume. Coprecipitation is thus a complex process, involving several mechanisms as a function of the P species and initial P/Fe ratio, and further contributing to the stabilization and selective accumulation of *myo*InsP6 in soil with respect to other organic P forms.

Keywords: Ferrihydrite, Surface adsorption, Phosphate, Inositol hexaphospate, Phosphatidylcholine, Surface properties.

Abbreviations: Fh (ferrihydrite), Pi (inorganic phosphate), *myo*InsP6 (*myo*-inositol hexaphosphate), PC (phosphatidylcholine).

1. Introduction

The composition and dynamics of organic phosphorus (P) in soil systems are strongly linked to the chemical characteristics and microbial degradation rate of plant residues, which control the availability of free phosphate for plants (Baldwin et al., 2005). The stabilization of organic P compounds by interaction with the mineral phase hampers their biodegradation and consequently strongly affects the biological cycling of P (Celi and Barberis, 2004; George et al., 2007; Giaveno et al., 2010). In general, these abiotic processes, involving adsorption and precipitation, are related to the different affinity of organic P compounds for iron (Fe) and aluminium (Al) species and to the solubility of their salts (Celi et al., 2003; Ognalaga et al., 1994; Zhang et al., 1994). This leads to the selective enrichment of inositol phosphates in soil with respect to more labile P monoesters and diesters, such as glucose-1-phosphate, DNA fragments or phosphoglycerides (Darch et al., 2014; George et al., 2018; Magid et al., 1996). Moreover, precipitation of inositol phosphates with other ions (such as Ca^{2+} and Mg^{2+}) can lead to a further retention and stabilization of these compounds (Anderson, 1963; Celi et al., 2000).

In addition to adsorption and precipitation, P retention through co-precipitation with Fe due to changes in pH, redox potential or ionic strength is a common process occurring in water and sediment environments. The oxidation of Fe(II), released into solution during mineral weathering and/or reductive dissolution under anoxic conditions, and precipitation of Fe (hydr)oxides is indeed known to contribute significantly to the retention of phosphate (Senn et al., 2015; van der Grift et al., 2016; Voegelin et al., 2010; 2013) and other inorganic and organic anions (Gorra et al., 2012; Mikutta et al., 2014; Senn et al., 2015). However, little is still known about the mechanisms of organic P retention during coprecipitation. As for the retention of organic compounds (Kleber et al., 2015), coprecipitation of organic P may involve different mechanisms, namely inclusion within the crystal structure, occlusion or physical entrapment within the growing crystal, as well as adsorption on neoformed amorphous to poorly crystalline nanoscale Fe (hydr)oxides. The extent and mechanisms of retention by coprecipitation are expected to be strongly dependent on the chemical structure of organic P and its relative abundance with respect to Fe. The retention of anions (e.g. organic matter, arsenate,

phosphate) coprecipitated with Fe (hydr)oxides was indeed reported to depend on the initial anion/Fe ratio in solution (Sodano et al., 2017; Thibault et al., 2009; Voegelin et al., 2010; 2013). For instance, phosphate was found to be incorporated into the newly formed Fe(III)-precipitates up to an initial P/Fe ratio of ~0.5-0.6 under varying experimental conditions of pH and background electrolytes (Châtellier et al., 2013; van der Grift et al., 2016; Voegelin et al., 2013), causing a much greater retention than that determined by adsorption. The presence of phosphate and the P/Fe ratio was also shown to slow down the kinetics of Fe(II) oxidation and Fe(III) precipitation (Mao et al., 2011; Mitra and Matthews, 1985; van der Grift et al., 2016), but to date no studies have addressed the kinetics of Fe(II) oxidative precipitation in the presence of P monoesters and diesters.

In addition, the presence of phosphate, silicate and other anions during Fe(III) precipitation was reported to interfere with Fe polymerization, mineral crystallization, spatial organization and to affect particles morphology and surface characteristics of the newly formed associations (Châtellier et al., 2004; 2013; Senn et al., 2015; Voegelin et al., 2013). The degree of crystallinity, the distortion of the crystal lattice and changes in the surface properties also depend on the initial P/Fe ratio. Thibault et al. (2009), for instance, showed that the presence of phosphate, even at low concentrations, inhibited the formation of the more crystalline 6L-ferrihydrite in favour of the less crystalline 2L-ferrihydrite, due to the perturbing effect of the anion incorporated into the particle structure during coprecipitation. Similarly, Voegelin et al. (2013) found that the precipitate changed from mostly poorly-crystalline lepidocrocite in the absence of phosphate to amorphous Fe phosphate at greater dissolved P/Fe ratios. Organic P compounds may affect coprecipitation processes differently with respect to inorganic phosphate as a function of their chemical structure, in particular steric hindrance and electric charge density. Mikutta et al. (2014), studying coprecipitation of Fe with organic matter, showed in fact that the initial C/Fe ratio induced differences in the functional composition of organic compounds at the particle interfaces due to the varying extent of competition between individual organic components.

This study aims at providing new insights into the role of coprecipitation in organic P retention through the evaluation of reaction kinetics and properties of the formed Fe-P coprecipitates. Based on previous considerations, we hypothesized that: (i) coprecipitation retains more P than adsorption; (ii)

the kinetics of P retention and Fe(II) oxidative precipitation depend on the type of organic P compound involved and the initial P/Fe ratio; (iii) the type of organic P compound influences the mineralogy, morphology and surface properties of the formed coprecipitates. We tested these hypotheses by synthesizing a series of Fe-P coprecipitates with increasing P/Fe ratios at near neutral pH. These systems were obtained during oxidative Fe(II) precipitation in the presence of three different P-containing compounds: a monoester, i.e. potassium *myo*-inositol hexaphosphate (*myo*InsP6), a diester, i.e. L-α-phosphatidylcholine (PC) or potassium dihydrogenphosphate (Pi). The three compounds were tested separately. For comparative purposes, we also studied the adsorption of these three compounds on a ferrihydrite synthesized by the same procedure.

2. Materials and methods

2.1 Inorganic and organic P compounds

All chemicals were analytical grade reagents from Sigma Aldrich: potassium phosphate monobasic, KH_2PO_4 (≥99.0%, P5655); dipotassium *myo*-inositol hexaphosphate ($C_6H_{16}O_{24}P_6K_2$, premium quality level, P5681); L-α-phosphatidylcholine from egg yolk (≥99.0%, lyophilized powder, P3556). To minimize the effect of hydrolysis, solutions of *myo*InsP6 and PC were freshly prepared prior to each test. All solutions were prepared in 0.01 M KCl. Dissolution of PC was facilitated by initially dissolving the phospholipid in ethanol.

2.2 Synthesis of ferrihydrite

Two-line ferrihydrite (Fh) was prepared by rapidly oxidizing a 2.0 mM $FeCl_2{\cdot}4H_2O$ solution at pH 6.0±0.2 in a 2 L reagent bottle fitted with an oxygen supply tube (200 ml min^{-1}), a pH probe and a burette tip. During oxidation, the contents were continuously stirred while pH was maintained at 6.0 by progressive addition of 0.25 M KOH by means of an automatic titrator (TTT85 titrator and ABU80 autoburette, Radiometer, Copenhagen, Denmark). The addition of base was constantly recorded during the experiment. After complete oxidation, evaluated through the disappearance of Fe(II) from solution, the reaction volume was reduced by centrifugation and removal of the supernatant, while the

concentrated suspension was stored at 4°C until further use. Fe concentration of the suspension was measured by atomic absorption spectrometry (PerkinElmer AAnalyst 1400, Norwalk, CT, USA) after acidic dissolution.

2.3 Synthesis of Fe-P adsorbed and coprecipitated systems

Ferrihydrite-P surface adsorbed systems (ADS) with increasing P loadings were prepared by mixing solutions of Pi, *myo*InsP6 and PC having different P concentrations (0.05-2 mM P) with suspensions of Fh (previously prepared as described above) at pH 6.0 to obtain initial solution molar P/Fe ratios [$(P/Fe)_0$] of 0.025, 0.05, 0.1 and 0.5 for PC and 0.05, 0.1, 0.5 and 1.0 for Pi and *myo*InsP6. $(P/Fe)_0$ ratios were chosen in accordance with the relative abundance and speciation of P compounds in soils (Magid et al., 1996) and based on the Langmuir adsorption coefficients (for Pi and *myo*InsP6) and Henry linear partitioning coefficients (for PC) determined by preliminary adsorption isotherm experiments (Table 1). Lower $(P/Fe)_0$ ratios were adopted for PC (between 0.025 and 0.5), based on its low water solubility and lower concentration in soils (Magid et al., 1996).

Fe-P coprecipitates (COP) with the same $(P/Fe)_0$ ratios as the adsorbed systems were prepared by oxidizing a 2 mM $FeCl_2 \cdot 4H_2O$ solution in the presence of increasing amounts of P, using the same procedure as described for the preparation of Fh above.

All batch preparations (2 l total volume) were performed in triplicate and maintained under vigorous stirring for 1 h at 25°C and subsequently allowed to equilibrate for 23 h at 4°C. The suspensions were then centrifuged (10,000 rpm for 10 min) and the supernatant analyzed for Fe, P and pH after filtration through a 0.20 μm nylon membrane filter. The amount of P retained was determined as the difference between initial and equilibrium P concentrations. The synthesized materials were washed with deionized water, dialyzed through a 14 kDa membrane, freeze-dried and stored in a desiccator until analysis.

2.4 Coprecipitation kinetics

During the synthesis of Fh and coprecipitates, a small aliquot of the suspension was sampled at regular time intervals, filtered through a 0.20 μm nylon membrane filter and analyzed to follow changes in the concentrations of Fe(II), Fe(III) and P over time. Dissolved Fe(II) concentrations were measured colorimetrically immediately after sampling using the 1,10-phenanthroline method (Loeppert and Inskeep, 1996) and the total Fe in the solution was measured by atomic absorption spectrometry (PerkinElmer AAnalyst 1400, Norwalk, CT, USA). Fe(III) concentrations were then calculated as the difference. Dissolved P concentrations were measured colorimetrically using the malachite green method (Ohno and Zibilske, 1991) for Pi while, for *myo*InsP6 and PC, dissolved P concentrations were measured colorimetrically after sulfuric-perchloric digestion (Martin et al., 1999). At each sampling time, the volume of OH^- added by the automatic titrator was recorded and used to calculate the H^+ ions released during Fe(II) oxidation and hydrolysis. All concentrations were corrected for the volume of KOH added and the change in the reaction volume with successive sampling.

2.5 Characterization of Fe-P adsorbed and coprecipitated systems

Iron and P contents in the obtained coprecipitates were determined by dissolving 1 mg of each sample in 2 ml of 6 M HCl, neutralizing with 10 M NaOH using 4-nitrophenol as pH indicator, and quantifying Fe and P concentrations as described above. The specific surface area (SSA) and porosity of the Fe-P systems were determined by N_2 adsorption-desorption isotherms performed at 77 K. The SSAs were estimated by applying the Brunauer-Emmett-Teller (BET) equation (Brunauer et al., 1938), whereas microporosity was calculated by the t-plot method (Gregg and Sing, 1982) and the mesopore size distribution by the Barrett-Joyner-Halenda (BJH) analysis (Barrett et al., 1951). The zeta potential (ζ) was calculated from the electrophoretic mobility determined on a suspension of 0.2 mL of freshly synthesized material diluted with 5 mL of its supernatant by Laser Doppler Velocimetry coupled with Photon Correlation Spectroscopy (LDV-PCS) using a spectrometer (DELSA 400, Beckman Coulter Inc., Hialeah, FL) equipped with a 5 mW He-Ne laser (632.8 nm). X-ray diffraction (XRD) pattern of powder samples were acquired in Bragg-Brentano geometry, using an X'Pert PRO MPD diffractometer (PANalytical, The Netherlands) equipped with Cu anode, ultrafast detector and working at 45 kV and

40 mA. The acquisition was performed between 10 and 80°, with a step size of 0.02° and a 3 s step time. Transmission electronic microscopy (TEM) was conducted in the bright field modality with a 300 kV ultrahigh resolution JEOL-JEM-3010 Transmission Electron Microscope (Tokyo, Japan), equipped with a LaB_6 filament and an Energy Dispersive X-ray Spectrometer (EDS) detector. Samples for TEM observations were prepared by depositing ground powder samples on a carbon coated copper grid (200 mesh). X-ray photoelectron spectroscopy (XPS) measurements were carried out using a PHI X-tool Automated XPS Microprobe (ULVAC-PHI, Inc., USA) applying monochromatic Al Kα-radiation. Samples were deposited on a double-stick tape that was placed on the sample holder. Except for drying the sample, no other pre-treatment was performed. For each sample, a survey scan was acquired. For Pi and *myo*InsP6 systems, narrow scans around the C 1s (278-298 eV), O 1s (523-543 eV), P 2p (123-143 eV) and Fe $2p_{3/2}$ (702-727 eV) were acquired. In the case of PC, also a narrow scan around the N 1s (370-450 eV) was acquired, in addition to the aforementioned elements. The XPS survey spectra confirmed the presence of P, O, Fe and C in all samples. N was also detected in the PC samples. Before determining the position of the peaks, a background subtraction was performed and the spectra were calibrated to C 1s excitation at BE of 284.8 eV from adventitious C, which was present on all surfaces. Data were collected and analyzed with the Multipack Software from Physical Electronics. Diffuse reflectance infrared (DR-IR) spectra were acquired between 4000 and 400 cm^{-1} at a resolution of 4 cm^{-1} with a Bruker Vertex 80v vacuum FT-IR Spectrometer (Bruker Scientific Instruments, Billerica, MA, USA) and a praying mantis diffuse reflectance attachment (Harrick Sci., Inc.). All samples were ground and prepared by mixing 10 mg of sample with 390 mg of finely powdered KBr (Merck, spectroscopic grade).

3. Results

3.1 P retention by adsorption and coprecipitation

Inorganic phosphate retention by adsorption on Fh increased with increasing $(P/Fe)_0$, gradually approaching a maximum of P/Fe ~ 0.20 at the largest $(P/Fe)_0$ ratio (Fig. 1). In contrast, molar P/Fe ratios of coprecipitates increased nearly linearly with increasing $(P/Fe)_0$, up to a maximum value of

0.78 over the experimental range evaluated. Adsorption of *myo*InsP6 also approached a maximum P/Fe ratio of around 0.25, while the similarity between coprecipitate P/Fe and $(P/Fe)_0$ ratios suggested a complete retention of *myo*InsP6 over the entire experimental range (Fig. 1). Retention of PC increased to P/Fe ratios of about 0.30 and 0.40 in the adsorbed and coprecipitated systems, respectively, at $(P/Fe)_0$ ratios of 0.5 (Fig. 1).

3.2 Coprecipitation kinetics

In the absence of P, the disappearance of Fe(II) from solution during oxidation at pH 6.0 was complete within 20 min (Fig. 2a). The release of H^+ followed a similar trend with a final H^+/Fe_0 ratio (Fig. 2b) that was only slightly greater than the stoichiometric value for the oxidation and hydrolysis of Fe^{2+} ($H^+/Fe_0 = 2.0$).

The presence of Pi slowed down the rate of Fe(II) oxidation and precipitation particularly at $(P/Fe)_0 = 0.1$ and the complete disappearance of Fe(II) occurred after approximatively 30 min (Fig. 3a). The rate of disappearance of Pi from the solution also tended to decrease with increasing $(P/Fe)_0$ (Fig. 3b). Whereas all the added anion was precipitated by the end of the oxidation at $(P/Fe)_0 \leq 0.5$, only 62% of initial Pi was retained by the end of the coprecipitation at $(P/Fe)_0 = 1.0$. The molar H^+/Fe_0 ratio at the end of the coprecipitation was > 2.0 for $(P/Fe)_0 < 0.5$, while it tended towards 1.5 at greater $(P/Fe)_0$ values (Fig. 3c).

The rate of Fe(II) oxidation and precipitation increased in the presence of *myo*InsP6, leading to a complete disappearance of Fe(II) from solution within only 10 min (Fig. 3d). The precipitation of *myo*InsP6 was also very rapid and complete, with all P disappearing from solution within the first 5 min for all $(P/Fe)_0$ ratios (Fig. 3e). The H^+/Fe_0 ratios at the end of the oxidation reached values around 2.1-2.3 in the two systems with lower $(P/Fe)_0$, while it tended towards approximately 1.5 and 1.0 for $(P/Fe)_0$ of 0.5 and 1.0, respectively (Fig. 3f).

The presence of PC did not influence the rate of Fe(II) oxidation and precipitation across all $(P/Fe)_0$ ratios, with rates similar to that obtained for the P-free system (Fig. 3g). The precipitation of P was also very rapid and complete, with P/P_0 values approaching unity within the first 5-10 min of

oxidation, irrespective of P loadings (Fig. 3h). Similarly, the production of protons during coprecipitation in the presence of PC was not influenced by the initial P concentration, and H^+/Fe_0 ratios tended towards 2.2 across all $(P/Fe)_0$ ratios (Fig. 3i).

3.3 Properties of the Fe-P precipitates

3.3.1 Surface properties

Coprecipitates obtained at increasing additions of Pi showed a consistent decrease in N_2-SSA, in contrast to the adsorbed systems that only presented a modest variation in N_2-SSA with increasing P loadings (Table 2). According to the IUPAC classification of adsorption isotherms (Alothman, 2012), all synthesized materials appeared to be mesoporous. In particular, Pi coprecipitates showed a great increase in pore volume with increasing $(P/Fe)_0$ (Table 2). At low $(P/Fe)_0$, pores were 7 to 10 nm wide (mesoporous material), while at greater P contents the pore width increased reaching a value of around 60 nm (macroporous material). In contrast, adsorbed Pi samples showed little variation in BET N_2-SSA, pore size and distribution, with an increase in the pore width (from 10 to 15 nm) only observed at the highest $(P/Fe)_0$ ratio. The ζ potentials of the Fe-Pi systems became less positive with increasing P contents, reaching negative values at $(P/Fe)_0$ 1.0 (Table 2). Similar ζ potentials were obtained for coprecipitated and adsorbed systems, despite the greater P contents in the former (Fig. 1).

At the lowest $(P/Fe)_0$ ratios, coprecipitation or adsorption of *myo*InsP6 induced a more prominent reduction in N_2-SSA in comparison with Pi, while similar values were observed at greater $(P/Fe)_0$ ratios (Table 2). Fe-*myo*InsP6 coprecipitates generally showed lower N_2-SSA values with respect to the adsorbed systems. Mesopore volumes were generally greater in the former, with the highest pore width (60 nm) observed already at $(P/Fe)_0 = 0.5$, while in the adsorbed systems pore volume and width tended to increase with increasing P loading over the whole $(P/Fe)_0$ range evaluated. Adsorption of *myo*InsP6 also led to a negative surface charge even at the lowest P loadings, while only coprecipitates obtained with $(P/Fe)_0 \geq 0.5$ showed negative ζ potentials.

Retention of PC by both adsorption and coprecipitation resulted in a drastic reduction in N_2-SSA and pore volumes even at the lowest $(P/Fe)_0$ values (Table 2). All systems showed positive surface charges with ζ potentials increasing to +33-34 mV at $(P/Fe)_0 = 0.05$ and then decreasing with increasing P loading approaching neutrality at the highest $(P/Fe)_0$ ratio. In the presence of the phospholipid, porosity was observed only at the lowest $(P/Fe)_0$ ratio in both adsorbed and coprecipitated systems, comparable to the value obtained for the P-free Fh. At the highest PC loadings, porosity was no longer detectable (Table 2).

3.3.2 X ray diffraction

The diffractograms of the adsorbed Pi systems showed two broad signals at around 36° and 63° 2θ, typical of 2-line Fh (Fig. 4). Coprecipitation with Pi resulted in a similar 2L-Fh pattern at low $(P/Fe)_0$, while at greater ratios diffractograms were characterized by a broad peak at 30° 2θ and no reflections at higher diffraction angles. Similar patterns were observed for adsorbed and coprecipitated *myo*InsP6 systems, with coprecipitates at higher $(P/Fe)_0$ values showing a single broad peak at around 30° 2θ. Both adsorbed and coprecipitated PC systems showed the two peaks of 2L-Fh across all $(P/Fe)_0$ ratios, although diffractograms of the systems synthesized at $(P/Fe)_0 \geq 0.1$ also showed an additional reflection at 20° 2θ.

3.3.3 IR spectroscopy

We focused the analyses of the IR spectra on the 1400-400 cm^{-1} region dominated by bands originating from P-O stretching and bending modes. The main P-O band of the Pi adsorbed systems, centred at $\simeq$ 1020 cm^{-1}, was asymmetric and composed of at least two overlapping bands (Fig. 5). The spectra of the coprecipitated systems showed similar features at the lowest $(P/Fe)_0$. However, this band became more symmetric and shifted from 1020 to 1050 cm^{-1} with increasing $(P/Fe)_0$.

The IR spectra of adsorbed *myo*InsP6 systems displayed three partly resolved bands at 1150, 1070 and 990 cm^{-1} (Fig. 5), assigned to υ_{as}(P-O), υ_s(P-O) and υ_{as}(P-O-C), respectively (Celi et al., 1999; Guan et al., 2006; Johnson et al., 2012). The same bands were also detected in the spectra of the

coprecipitated systems at $(P/Fe)_0 \leq 0.1$. At the greater ratios, the band at 1150 cm^{-1} disappeared and two low-intensity bands formed at 860 and 810 cm^{-1}, attributed to υ_{as}(C-O) and υ_s(C-O), respectively. The IR spectra of PC systems displayed pronounced and resolved bands at 1250 cm^{-1} (υ_{as} of P=O) and 1100 cm^{-1} (υ_{as} of P-O) and a mode involving the choline quaternary ammonium $C\text{-}N^{+}\text{-}(CH_3)_3$ group at 970 cm^{-1} (Fig. 5). These features confirmed that PC was not hydrolyzed during the experiments. Adsorbed and coprecipitated systems showed similar IR patterns, although differences in the absorption peaks related to the phosphate group were observed with increasing P loading. In particular, the systems at the two greater $(P/Fe)_0$ distinguished themselves from those at the two lower $(P/Fe)_0$ as the band at 1064 cm^{-1}progressively split into two bands and new bands at 930 and 870 cm^{-1} appeared.

3.3.4 XPS

Molar P/Fe ratios were calculated from surface element composition derived from XPS survey spectra (Table 2). Comparison with molar P/Fe ratios obtained by acid dissolution was used to evaluate surface enrichment of P during the synthesis of these systems. Adsorption of Pi, *myo*InsP6 and PC resulted in surface molar P/Fe ratios that were slightly greater than molar ratios obtained by acid dissolution, except for the adsorption of PC at high $(P/Fe)_0$ ratios, which showed an elevated P surface enrichment. Coprecipitation with Pi resulted in a surface enrichment of P particularly at high P loadings, and a similar surface P enrichment at high $(P/Fe)_0$ ratios was observed for the coprecipitation with *myo*InsP6, although to a lesser extent with respect to Pi. Coprecipitation with PC resulted in the highest enrichment of P on the surface with XPS P/Fe ratios as high as 9.18 (compared to 0.44 obtained by chemical analysis) at the highest P loading.

Fe $2p_{3/2}$ XPS spectra of adsorbed Pi systems showed a peak with a binding energy between 711 and 710 eV (Fig. 6), corresponding to a Fe(III)-oxide species (Moulder et al. 1995), in our case ferrihydrite. The intensity of this peak decreased with increasing P content, suggesting a major coating of P on the (hydr)oxide surface. The Fe $2p_{3/2}$ peak of Pi coprecipitates (Fig. 6) not only became less intense with increasing P loading, but also shifted from ~ 710 to ~ 712 eV, as a result of a change in Fe chemical

state. The P 2p detail spectra of both adsorbed and coprecipitated systems (the latter shown in Fig. 7) were fitted with a single peak centered at 133.5-134.1 eV, suggesting the existence of just one type of P compound in the structure with a binding energy characteristic of tetracoordinated phosphorus, as in phosphates (Amaral et al., 2005).

Similarly, in *myo*InsP6 adsorbed systems Fe signals showed a slight decrease in intensity with increasing P content with no peak shift (~ 710 eV), while the corresponding coprecipitates showed both a decrease in intensity and a shift in Fe $2p_{3/2}$ peaks, from 710 to 712 eV with increasing $(P/Fe)_0$ (Fig. 6).

In both adsorbed and coprecipitated PC systems, the intensity of the Fe $2p_{3/2}$ peak decreased drastically with increasing P content and Fe was not detected at the highest $(P/Fe)_0$ ratio (Fig. 6). A minor shift in the peak position to greater binding energies was visible, although within the range of 710-711 Ev, characteristic of the Fe oxide.

3.3.5 TEM

TEM images of Fh synthesized from the oxidation and hydrolysis of Fe^{2+} indicate that the (hydr)oxide is composed of particle aggregates that vary from 0.2 to 0.5 μm in size (Fig. 8). Particles appear quite small (2-5 nm), well defined and in some regions with an elongated form. TEM images of Pi coprecipitates showed an increase in particle size with increasing P content. At low $(P/Fe)_0$ the morphology was similar to the P-free Fh, and the systems appeared to be composed of an amorphous part and of some thin lath-like particles. At greater $(P/Fe)_0$, aggregates appeared to be more compact with bigger individual particles having poorly defined edges and smooth surfaces. Also in *myo*InsP6 coprecipitates aggregation increased with increasing P content with particles ranging from 1-3 nm to 5-10 nm at $(P/Fe)_0 = 0.05$ and 1.0, respectively. TEM images of PC coprecipitates showed few differences in morphology with increasing P contents. Even at the highest $(P/Fe)_0$ the particles were very small. Although the likely presence of a phospholipid layer on the surface of the (hydr)oxide led to more opaque TEM images, many elongated and acicular structures were visible.

4. Discussion

4.1 P retention and kinetics during coprecipitation

Coprecipitation generally led to a substantially higher retention of all three P forms compared to adsorption, particularly at greater $(P/Fe)_0$. Inorganic phosphate retained by coprecipitation at the highest P loading was about four times greater than that retained by adsorption. When present in solution at a molar $(P/Fe)_0 \leq 0.5$, the anion was completely removed from solution during coprecipitation (along the 1:1 line in Fig. 1), while up to 60% of Pi was retained at $(P/Fe)_0 = 1.0$, in accordance with the findings of Châtellier et al. (2013) and Voegelin et al. (2013). The presence of Pi slowed down the rate of Fe(II) oxidative precipitation, likely interfering with the formation of crystallization nuclei and subsequent precipitation of Fe (hydr)oxides. This is in agreement with van der Grift et al. (2016) who hypothesized that dissolved Pi might affect Fe(II) oxidation either by changing the speciation of dissolved Fe or by affecting the surface speciation of the Fe hydroxyphosphates. The latter may influence the nucleation of Fe precipitates and interfere with surface catalysis. A decrease in reaction rate was also observed in the presence of dissolved organic matter (Chen et al., 2014; Pédrot et al., 2011; Shimizu et al., 2013; Sodano et al., 2016), proteins (Kashyap et al., 2014) or other anions such as arsenate (Mikutta et al., 2014) and silicate (Voegelin et al., 2013). The faster disappearance of Pi from the solution with respect to Fe precipitation and H^+ release at $(P/Fe)_0 = 0.05$ suggests that Fe-phosphate nuclei were rapidly formed. However, the amount of H^+ released by the end of the reaction ($H^+/Fe_0 \approx 2.4$) was similar to that observed in the absence of P ($H^+/Fe_0 \approx 2.2$), suggesting that at low P loading Fe (hydr)oxide precipitation occurred (Eq.1) and Pi adsorption on the newly formed mineral surface was mainly responsible for P retention.

$$Fe^{2+} + 0.25O_2 + 1.5H_2O \rightarrow FeOOH_{(s)} + 2H^+ \quad \text{(Eq. 1)}$$

The slightly higher H^+/Fe_0 ratio obtained with respect to the theoretical stoichiometry may be due to other reactions, such as Fe(II) adsorption on the new formed surfaces and generation of reactive oxygen species (Jones et al., 2015), which may contribute to modify the production of protons.

At greater P concentrations the mechanisms involved changed and the precipitation of $FePO_4$ (Eq. 2) contributed significantly to P retention (Voegelin et al., 2013).

$$Fe^{2+} + 0.25O_2 + H_2PO_4^- \rightarrow FePO_{4(s)} + H^+ + 0.5H_2O \quad \text{(Eq. 2)}$$

In fact, at $(P/Fe)_0 \geq 0.5$ the measured final $H^+/Fe_0 \approx 1.6$ approached the theoretical stoichiometry of the combined reactions of $FePO_4$ precipitation and FeOOH formation (Eq. 3), in line with the observations of Châtellier et al. (2013):

$$2Fe^{2+} + 0.5O_2 + H_2PO_4^- + H_2O \rightarrow FeOOH_{(s)} + FePO_{4(s)} + 3H^+ \quad \text{(Eq. 3)}$$

These results suggest that Pi retention during coprecipitation at high P loadings mainly involved $FePO_4$ precipitation (up to 50% of the initial P), but the quantitative coprecipitation data (Fig. 1) highlighted also other mechanisms including adsorption on the newly formed Fe (hydr)oxide and/or inclusion into particle aggregates.

P retention during coprecipitation in the presence of *myo*-inositol hexaphosphate was up to five times greater than adsorption at the highest $(P/Fe)_0$, and total removal of the P compound was observed over the whole experimental range of $(P/Fe)_0$ values. In contrast to Pi, *myo*InsP6 tended to accelerate Fe(II) oxidative precipitation. An increase in the rate of Fe(II) oxidation has also been observed in the presence of other organic ligands, such as citrate (Pham and Waite, 2008), EDTA and fulvic acids (Jones et al., 2015), and is explained by the capacity of these ligands to form strong Fe(II) complexes with greater oxidation rate constants with respect to Fe(II). As *myo*InsP6 is known to have a higher Fe(II) complexation capacity than Pi (Celi and Barberis, 2004 and references therein) Fe-*myo*InsP6 species are expected to form rapidly. Considering the acid dissociation constants of the six phosphate groups (Table 3), *myo*InsP6 at pH 6 may be present as $[C_6H_6(HPO_4)_4(PO_4)_2]^{8-}$ and can thus chelate from one to four Fe(II) ions (Eq. 4):

$$nFe^{2+} + [C_6H_6(HPO_4)_4(PO_4)_2]^{8-} \rightarrow [Fe(II)_n{-}C_6H_6(HPO_4)_4(PO_4)_2]^{2n-8} \quad \text{(Eq. 4)}$$

This complex may favour the oxidation of Fe(II) in the presence of O_2 according to Eq. 5, and potentially act as crystallization nuclei for the further precipitation of Fe (hydr)oxides:

$[Fe(II)_n{-}C_6H_6(HPO_4)_4(PO_4)_2]^{2n-8} + 0.25nO_2 + nH^+ \rightarrow [Fe(III)_n{-}C_6H_6(HPO_4)_4(PO_4)_2]^{3n-8} + 0.5nH_2O$ (Eq. 5)

The H^+/Fe_0 ratio of 2.0 observed at the end of the coprecipitation at $(P/Fe)_0 \leq 0.1$ suggests that at low *myo*InsP6 concentrations P retention is determined by the oxidative precipitation of FeOOH and rapid sorption of *myo*InsP6 on the newly formed (hydr)oxide, although the formation and precipitation of Fe(III)-*myo*InsP6 species cannot be completely excluded. At greater *myo*InsP6 concentrations ($(P/Fe)_0 \geq 0.5$), the additional formation and precipitation of $[Fe(III)_4\text{-}C_6H_6(PO_4)_6]$ may contribute increasingly to the overall retention of P, leading to the observed decrease in final H^+/Fe_0 ratios from ~ 2.0 to ~ 1.5 and 1.0 for $(P/Fe)_0 = 0.5$ and 1.0, respectively. Measured proton release for the highest P loading may be hypothetically explained through the formation of FeOOH and Fe(III)-*myo*InsP6 in a stoichiometric ratio of 4:1 by the end of the oxidative precipitation of Fe(II), according to the reaction:

$$8Fe^{2+} + [C_6H_6(HPO_4)_4(PO_4)_2]^{8-} + 2O_2 + 4H_2O \rightarrow 4FeOOH + [Fe(III)_4{-}C_6H_6(PO_4)_6] + 8H^+ \quad \text{(Eq. 6)}$$

In this case, aside from Fe(III)-*myo*InsP6 precipitation, adsorption on FeOOH and inclusion into aggregates consistently contributed to the complete retention of *myo*InsP6.

Coprecipitation of phosphatidylcholine also led to the complete removal of the P compound from solution, with a slightly larger P retention than the adsorbed system at the highest $(P/Fe)_0$. However, in contrast to the other P species, the presence of the phospholipid did not affect Fe(II) kinetics. PC is an amphipathic molecule with a hydrophobic tail composed of fatty acid esters bound to glycerol, and a hydrophilic zwitterionic "head" containing a completely dissociated phosphate group (pK_a=0.8) and a protonated quaternary amine with three methyl groups (pK_a=11.25) at the working pH. The fact that the phosphate diester scarcely interfered with Fe(II) oxidative precipitation is likely because of the limited chelating capacity offered by the single negative group of phosphate. In addition, the repulsive forces imposed by the terminal quaternary amine group on the polar head could preclude direct contact between the phosphodiester group and the Fe(II) ions (Cagnasso et al., 2010; Xu et al., 2009). Thus, Fe(II) oxidative precipitation was not influenced by the presence of PC and the final H^+/Fe_0 ratio (≈ 2) did not deviate from the stoichiometric value (Eq. 1).

4.2 Properties of the Fe-P systems

The complementary surface, microscopic and spectroscopic analysis of this study showed that the mineralogy, structure and surface properties of the obtained coprecipitates differed markedly as a function of the P species and $(P/Fe)_0$ ratios

4.2.1 Pi coprecipitates

Aggregative processes occurring during coprecipitation, favoured by the attraction between the negatively charged P anions and the positively charged, newly formed, Fe (hydr)oxide surfaces, were probably responsible for the reduction in N_2-SSA and increase in mesopore volume observed in the presence of Pi. Nanoparticle coprecipitates with a short-range crystalline order were formed at low Pi concentrations, evidenced by the smooth surface texture and broad nature of the XRD peaks (Eusterhues et al., 2008; Janney et al., 2000; Jia et al., 2007), and were very similar to those obtained from P-free solutions. Châtellier et al. (2004) hypothesized that during the synthesis of $FePO_4$ systems, the phosphate ligand was likely competing with ferrous ions for adsorption on the lateral planes of the growing crystals resulting in the inhibition of particle growth. The ζ potential measured at $(P/Fe)_0 \leq 0.5$ suggested that the positively charged surface of the Fe (hydr)oxide at pH 6.0 was only partially balanced by the dissociated phosphate groups at this pH (Celi et al., 2001). However, surface P/Fe ratios obtained by XPS, approximately two times greater than those obtained by chemical analysis, suggest that phosphate groups were nonetheless enriched at the surface, possibly due to the adsorption on the lateral planes of the growing FeOOH crystals (Châtellier et al., 2004),

Increasing P loading led to the formation of more spherical-like particles, consistent with the formation of Fe(III)-phosphates (Kaegi et al., 2010). This was in line with the lower amount of protons released during Fe(II) oxidation and hydrolysis ($H^+/Fe_0 < 2$), and the progressive broadening and disappearance of the main XRD peaks of 2L-Fh, together with the appearance of the reflection at 30° 2θ of amorphous Fe(III)-phosphate (Lai et al., 2011; Voegelin et al., 2013). In addition, the shift in Fe binding energy from ~ 710 to 712 eV with increasing $(P/Fe)_0$ reflects a change in Fe chemical state from an oxide-like structure to a Fe-phosphate salt (Mallet et al., 2013). Indeed, Grosvernor et al.

(2004) found that the binding energy associated with Fe (ferrous or ferric) $2p_{3/2}$ peak increases with an accentuation in the ionic bond character between Fe and the ligand, due to the reduction in shielding of the Fe cation by the more electronegative ligands. This effect was not observed in the adsorbed Pi systems, as no change in the chemical state of Fe is expected. Although the contribution of $FePO_4$ precipitation to Pi retention clearly increased with increasing $(P/Fe)_0$, the negative surface charge at the highest P loading (−11 mV) was much lower than that of pure $FePO_4$ (Li and Standforth, 2000) and closer to that of the adsorbed systems, further indicating that Pi adsorption on the newly formed hydroxide surfaces contributed to total P retention. Additional insights into the retention and nature of interaction between Fe and Pi during adsorption and coprecipitation were obtained by the IR spectra. Adsorption of Pi onto iron octahedral structures at the Fh surface was highlighted by the difference between the peak maxima of the solution P species and the adsorbed ones, confirming the formation of P inner-sphere complexes (Arai and Sparks, 2001). Given the amorphous nature of the substrate, the presence of multiple (slightly) different phosphate complexes at the ferrihydrite surface is not unlikely and leads to a larger variety in the characteristics of surface sites available for phosphate adsorption than in the case of a crystalline oxide such as goethite or haematite (Elzinga and Sparks, 2007), resulting in less symmetrical peaks. The similarity between the IR spectra of the adsorbed systems and of the low $(P/Fe)_0$ coprecipitates suggests that, although during coprecipitation Fe(III)-phosphate formed first, the final product is characterized by the presence of phosphate accumulated on the surface, in line with XPS results. This is in agreement with Voegelin et al. (2013), who suggested a transformation of Fe(III)-phosphate into P-ferrihydrite during Fe(II) oxidation at $(P/Fe)_0 < 0.5$. The one featured peak obtained at greater $(P/Fe)_0$ confirms the formation of the phosphate salt. In addition, under most conditions, Fe(III)-phosphate contains the non-protonated phosphate ion, justifying the broad features centred consistently around 1150-1050 cm^{-1} (Persson et al., 1996).

4.2.2 *myo*InsP6 coprecipitates

Similarly to Pi, coprecipitation in the presence of increasing concentrations of *myo*InsP6 led to a reduction in N_2-SSA and an increase in mesopore volume. Coprecipitates formed in the presence of *myo*InsP6 at low $(P/Fe)_0$ ratios were mainly constituted of ferrihydrite particles (1-2 nm) with some needles and laths probably due to lepidocrocite. In contrast to the adsorbed systems that showed a negative surface charge even at the lowest P loadings, the surface charge of coprecipitates unexpectedly remained highly positive, suggesting that the high charge density of *myo*InsP6 was partially neutralized (Celi and Barberis, 2004). This, together with the kinetic features, may support the hypothesis that Fe(III)-*myo*InsP6 species could act as nuclei of crystallization accelerating crystal growth on lateral planes, while including the organic P compound within the structure.

At the highest $(P/Fe)_0$ ratios the particles were more aggregated, albeit the negative charge of the particle surface and the strong colloidal dispersion effect exerted by *myo*InsP6 (Celi et al., 1999; Wan et al., 2016). This may suggest that, as for Pi, simultaneous precipitation of Fe hydroxides and Fe-*myo*InsP6 salts may occur, as well as adsorption of *myo*InsP6 on the newly formed oxide surfaces. The latter may be followed by the further formation of ternary systems with Fe(III), partially neutralizing *myo*InsP6 charge. This can also be deduced from XR diffractograms, showing a progressive broadening and disappearance of the 2L-Fh signals and the appearance of a single signal attributed to the formation of Fe(III)-*myo*InsP6 (Yan et al., 2014). The shift in Fe binding energy in the XP spectra confirmed a change from a Fe-O to a Fe-P like bonding type (Mallet et al., 2013). A stronger association of Fe and P atoms of *myo*InsP6 than that found within the structure of some Fe-inorganic P precipitates by EXAFS studies (Châtellier et al., 2013; Senn et al., 2015) could be expected due to its unique affinity for Fe (Martin and Evans, 1987). IR spectra suggest that, during adsorption, the phosphate groups of *myo*InsP6 coordinated with metal ion(s) at the hydroxide surface by forming inner-sphere complexes, as the bands corresponding to the vibration of phosphate groups split into two or three bands, and shifted with respect to those of the free compound in solution (Celi et al., 1999; Guan et al., 2006). The inner-sphere complexes formed via ligand exchange of aquo- and hydroxo-groups can involve a different number of phosphate groups depending on the oxide (Celi et al., 1999Yan et al., 2014). The three featured absorption band is again similar in the low $(P/Fe)_0$

coprecipitates, confirming that adsorption on the forming surface dominated Fe(III)-*myo*InsP6 precipitation, as also deduced by XRD and XPS data.

4.2.3 PC coprecipitates

An even stronger effect on sample morphology was observed in both adsorbed and coprecipitated PC systems, where, except for $(P/Fe)_0 = 0.025$, the N_2-SSA was drastically reduced and pores occluded with increasing P concentration. PC may also inhibit crystallization due to the adsorption to nucleation sites, as observed for citrate (Liu and Huang, 2003), and lead to a substantial particle aggregation. Mikutta et al. (2008) obtained comparable features with exopolysaccharides. The strong similarity between coprecipitated and adsorbed systems further confirms that the two processes were not very different. Even in the presence of PC, Fe(II) was oxidized and precipitated to form a 2-line Fh onto which PC was mainly retained by a solid/liquid partitioning, without changes in the oxidation and precipitation kinetics and stoichiometry. The accumulation of the phospholipid on the surface was also supported by the TEM images where the material appeared blurred and opaque, as observed with other lipids (Ge et al., 2003; Yanyu et al., 2006). The positive charge of the particles at the lower $(P/Fe)_0$ suggests that PC may approach the Fe(III) hydroxide by the phosphate group leaving the $-N(CH_3)^+$ moiety more exposed to the aqueous medium (Denizot et al., 1999). At the highest $(P/Fe)_0$ ratio the nearly neutral surface charge of the coprecipitates indicates a self-assembly of the phospholipid with the formation of a bilayer. De Cuyper and Joniau (1991) proposed that phospholipids are presumably adsorbed on Fe_3O_4 surfaces in the form of vescicles, through an "aqueous transfer mechanism", by which the molecules escaped from the vesicles, rapidly passed through the water phase and were retained by the oxide, forming a bilayer. This may be further confirmed by the XRD peak at 20° 2θ of both adsorbed and coprecipitated systems at the highest $(P/Fe)_0$, attributable to the presence of an ordered phosphatidylcholine layer (Hou et al., 2013; Yang et al., 2012). Xu et al. (2009) reported that the self-assembly and formation of phospholipid bilayers was found to be oxide-dependent and occurred mostly on positively charged mineral surfaces. The formation of a bilayer may completely mask the Fe hydroxide surface, forming a >10 nm thick layer

and preventing Fe from being detected and quantified by XPS. The interaction of PC with Fe produced slight modifications in the IR spectra of the phospholipid with increasing P loadings in both adsorbed and coprecipitated systems. This may confirm that PC was retained by the formed Fe hydroxide only by weak non-specific forces (Xu et al., 2009). Upon adsorption of a phosphatidylcholine on goethite, Cagnasso et al. (2010) also observed a strong shift of the $-CH_2-COOR$ -methylene vibrations, suggesting a conformation change to a more crystalline state. This was not detected in our spectra, although the formation of an ordered bilayer was deduced by XRD and surface charge features.

5. Conclusions

Coprecipitation resulted in a significantly greater P retention with respect to adsorption for all the three P compounds studied, particularly at high initial $(P/Fe)_0$ ratios. Fe^{2+} oxidative precipitation in the presence of low Pi concentrations was slowed down with respect to P-free ferrihydrite precipitation, probably due to the interference and poisoning of the anion with the (hydr)oxide crystallization nuclei, leading to the formation of small nanometric particles. At greater Pi concentrations, particles were more aggregated, with a lower surface area and increased porosity, likely due to the simultaneous salt precipitation and (hydr)oxide formation.

Conversely to Pi, the presence of *myo*InsP6 accelerated Fe(II) oxidation and precipitation through the fast formation of more easily oxidable Fe-*myo*InsP6 complexes, as testified by the immediate disappearance of P from the solution. The presence of more phosphate groups in the same molecule could favour the growth of Fe oxides in more directions, leading to systems bearing *myo*InsP6 more inside the structure with respect to Pi coprecipitates. Nevertheless, as for Pi, at low *myo*InsP6 concentration the adsorption on the forming surface seemed to dominate over the precipitation of the salt and remains a relevant mechanism even at high *myo*InsP6 concentration.

By contrast, PC did not cause any variation in Fe(II) oxidation and precipitation kinetics, even with increasing $(P/Fe)_0$, with the formation of a 2L-Fh at any PC concentration and physical partitioning of the organic P compound on the surface of the obtained (hydr)oxide. The presence of increasing PC

concentrations on ferrihydrite surface led to a sharp decrease of N_2-SSA and total pore volume, both for the coprecipitated and adsorbed systems.

Coprecipitation of soluble organic P compounds during Fe(II) oxidation is therefore a much more complex process than adsorption, occurring through several mechanisms and with different kinetics depending mostly on P species and $(P/Fe)_0$ ratio. The type and initial concentration of P may indeed lead to the formation of Fe(III)-coprecipitates with different surface properties which can in turn affect their reactivity at the solid/solution interface. The larger P retention and the different morphological and mineralogical features of coprecipitates obtained with *myo*InsP6 compared to PC and Pi may further increase its stabilization and selective accumulation in soil while reducing P bioavailability, although additional investigation should be carried out to evaluate the stability and transformation of these coprecipitates in the short and long term and following alternating redox conditions.

References

Alothman, Z.A., 2012. A review: fundamental aspects of silicate mesoporous materials. Materials. 5, 2874-2902.

Amaral, I.F., Granja, P.L., Barbosa, M.A., 2005. Chemical modification of chitosan by phosphorylation: an XPS, FT-IR and SEM study. J. Biomater. Sci. Polym. Ed. 16(12), 1575-1593.

Anderson, G., 1963. Effect of iron/phosphorus ratio and acid concentration on the precipitation of ferric inositol hexaphosphate. J. Sci. Food Agric. 14(5), 352-359.

Arai, Y., Sparks, D.L., 2001. ATR-FTIR spectroscopic investigation on phosphate adsorption mechanisms at the ferrihydrite-water interface. J. Colloid Interface Sci. 214(2), 317-326.

Baldwin, D.S., Howitt, J.A., Beattie, J.K., 2005. Abiotic degradation of organic phosphorus compounds in the environment, in: Turner, B.L., Frossard, E., Baldwin, D.S. (Eds.), Organic phosphorus in the environment. CABI Publishing, Wallingford, UK, pp. 75–88.

Barrett, E.P., Joyner, L.G., Halenda, P.P., 1951. The determination of pore volume and area distribution in porous substances. I. Computations from Nitrogen isotherms. J. Am. Chem. Soc. 73(1), 373-380.

Brunauer, S., Emmett, P.H., Teller, E., 1938. Adsorption of gases in multimolecular layers. J. Am. Chem. Soc. 60(2), 309-319.

Cagnasso, M., Boero, V., Franchini, M.A., Chorover, J., 2010. ATR-FTIR studies of phospholipid vesicle interactions with α-FeOOH and α-Fe_2O_3 surfaces. Colloids Surf., B. 76(2), 456-467.

Celi, L., Lamacchia, S., Ajmone-Marsan, F., Barberis, E., 1999. Interaction of inositol hexaphosphate on clays: Adsorption and charging phenomena. Soil Sci. 164(8), 574-585.

Celi, L., Lamacchia, S., Barberis, E., 2000. Interaction of inositol phosphates with calcite. Nutr. Cycl. Agroecosys. 57(3), 271-277.

Celi, L., Presta, M., Ajmone-Marsan, F., Barberis, E., 2001. Effects of pH and electrolytes on inositol hexaphosphate interaction with goethite. Soil Sci. Soc. Am. J. 65(3), 753-760.

Celi, L., De Luca, G., Barberis, E., 2003. Effects of interaction of organic and inorganic P with ferrihydrite and kaolinite-iron oxide systems on iron release. Soil Sci. 168(7), 479-488.

Celi, L., Barberis, E., 2004. Abiotic stabilization of organic phosphorus in the environment, in: Turner, B.L., Frossard, E., Baldwin, D.S. (Eds.), Organic phosphorus in the environment. CABI Publishing, Wallingford, UK, pp. 113–132.

Châtellier, X., West, M.M., Rose, J., Fortin, D., Leppard, G.G., Ferris, F.G., 2004. Characterization of iron-oxides formed by oxidation of ferrous ions in the presence of various bacterial species and inorganic ligands. Geomicrobiol. J. 21(2), 99-112.

Châtellier, X., Grybos, M., Abdelmoula, M., Kemner, K.M., Leppard, G.G., Mustin, C., West, M.M., Paktunc, D., 2013. Immobilization of P by oxidation of Fe(II) ions leading to nanoparticle formation and aggregation. Appl. Geochem. 35, 325-339.

Chen, C., Dynes, J.J., Wang, J., Sparks, D.L., 2014. Properties of Fe-organic matter associations via coprecipitation versus adsorption. Environ. Sci. Technol. 48(23), 13751-13759.

Corbridge, D.E.C., 1985. Phosphorus: An outline of its chemistry, biochemistry and technology. Elsevier, Amsterdam, 761 pp.

Costello, A.J.R., Glonek, T., Myers, T.C., 1976. ^{31}P nuclear magnetic resonance: pH titrations of *myo*-inositol hexaphosphate. Carbohyd. Res. 46(2), 159-171.

Darch, T., Blackwell, M.S.A., Hawkins, J.M.B., Haygarth, P.M., Chadwick, D., 2014. A meta-analysis of organic and inorganic phosphorus in organic fertilizers, soils and water: Implications for water quality. Crit. Rev. Env. Sci. Tec. 44(19), 2172-2202.

De Cuyper, M., Joniau, M., 1991. Mechanistic aspects of the adsorption of phospholipids onto lauric acid stabilized magnetite nanocolloids. Langmuir. 7(4), 647-652.

Denizot, B., Tanguy, G., Hindre, F., Rump, E., Le Jeune, J.J., Jallet, P., 1999. Phosphorylcholine coating of iron oxide nanoparticles. J. Colloid Interface Sci. 209(1), 66-71.

Elzinga, E.J., Sparks, D.L., 2007. Phosphate adsorption onto hematite: An in-situ ATR-FTIR investigation of the effects of pH and loading level on the mode of phosphate surface complexation. J. Colloid Interface Sci. 308(1), 53-70.

Eusterhues, K., Wagner, F.E., Häusler, W., Hanzlik, M., Knicker, H., Totsche, K.U., Kögel-Knabner, I., Schwertmann, U., 2008. Characterization of ferrihydrite-soil organic matter coprecipitates by X-ray diffraction and Mössbauer spectroscopy. Environ. Sci. Technol. 42(21), 7891–7897.

Ge, L., Möhwald, H., Li, J., 2003. Phospholipid liposomes stabilized by the coverage of polyelectrolyte. Colloids Surf., A. 221(1-3), 49-53.

George, T.S., Simpson, R.J., Hadobas, P.A., Marshall, D.J., Richardson, A.E., 2007. Accumulation and phosphatase-lability of organic phosphorus in fertilised pasture soils. Aust. J. Agric. Res. 58(1), 47-55.

George, T.S., Giles, C.D., Menezes-Blackburn, D., Condron, L.M., Gama-Rodrigues, A.C., Jaisi, D., Lang, F., Neal, A.L., Stutter, M.I., Almeida, D.S., Bol, R., Cabugao, K.G., Celi, L., Cotner, J.B., Feng, G., Goll, D.S., Hallama, M., Krueger, J., Plassard, C., Rosling, A., Darch, T., Fraser, T., Giesler, R., Richardson, A.E., Tamburini, F., Shand, C.A., Lumsdon, D.G., Zhang, H., Blackwell, M.S.A., Wearing, C., Mezeli, M.M., Almås, Å.R., Audette, Y., Bertrand, I., Beyhaut, E., Boitt, G., Bradshaw, N., Brearley, C.A., Bruulsema, T.W., Ciais, P., Cozzolino, V., Duran, P.C., Mora, M.L., de Menezes, A.B., Dodd, R.J., Dunfield, K., Engl, C., Frazão, J.J., Garland, G., González Jiménez, J.L., Graca, J., Granger, S.J., Harrison, A.F., Heuck, C., Hou, E.Q., Johnes, P.J., Kaiser, K., Kjær, H.A., Klumpp, E., Lamb, A.L., Macintosh, K.A., Mackay, E.B., McGrath, J., McIntyre, C., McLaren, T., Mészáros, E., Missong, A., Mooshammer, M., Negrón, C.P., Nelson, L.A., Pfahler, V., Poblete-Grant, P., Randall, M., Seguel, A., Seth, K., Smith, A.C., Smits, M.M., Sobarzo, J.A., Spohn, M., Tawaraya, K., Tibbett, M., Voroney, P., Wallander, H., Wang, L., Wasaki, J., Haygarth, P.M., 2018. Organic phosphorus in the terrestrial environment: A perspective on the state of the art and future priorities. Plant Soil. 427, 191-208.

Giaveno, C., Celi, L., Richardson, A.E., Simpson, R.J., Barberis, E., 2010. Interaction of phytases with minerals and availability of substrate affect the hydrolysis of inositol phosphates. Soil Biol. Biochem. 42(3), 491-498.

Gorra, R., Webster, G., Martin, M., Celi, L., Mapelli, F., Weightman, A.J., 2012. Dynamic microbial community associated with iron-arsenic co-precipitation products from a groundwater storage system in Bangladesh. Microb. Ecol. 64(1), 171-186.

Gregg, S.J., Sing, K.S.W., 1982. Adsorption, surface area and porosity. Academic Press, London.

Grosvernor, A.P., Kobe, B.A., Biesinger, M.C., McIntyre, N.S., 2004. Investigation of multiplet splitting of Fe 2p XPS spectra and bonding in iron compunds. Surf. Interface Anal. 36(12), 1564-1574.

Guan, X.H., Shang, C., Zhu, J., Chen, G.H., 2006. ATR-FTIR investigation on the complexation of myo-inositol hexaphosphate with aluminum hydroxide. J. Colloid Interface Sci. 293(2), 296-302.

Hou, Z., Li, Y., Huang, Y., Zhou, C., Lin, J., Wang, Y., Cui, F., Zhou, S., Jia, M., Ye, S., Zhang, Q., 2013. Phythosomes loaded with mitomycin C-soybean phosphatidylcholine complex developed for drug delivery. Mol. Pharmaceutics. 10(1), 90-101.

Janney, D.E., Cowley, J.M., Busek, P.R., 2000. Transmission electron microscopy of synthetic 2- and 6-line ferrihydrite. Clays Clay Miner. 48(1), 111 - 119.

Jia, Y., Xu, L., Wang, X., Demopoulos, G.P., 2007. Infrared spectroscopic and X-ray diffraction characterization of the nature of adsorbed arsenate on ferrihydrite. Geochim. Cosmochim. Acta. 71(7), 1643–1654.

Johnson, B.B., Quill, E., Angove, M.J., 2012. An investigation of the mode of sorption of inositol hexaphosphate to goethite. J. Colloid Interface Sci. 367(1), 436-442.

Jones, A.M., Griffin, P.J., Waite, T.D., 2015. Ferrous iron oxidation by molecular oxygen under acidic conditions: The effect of citrate, EDTA and fluvic acid. Geochim. Cosmochim. Acta. 160, 117-131.

Kaegi, R., Voegelin, A., Folini, D., Hug, S.J., 2010. Effect of phosphate, silicate and Ca on the morphology, structure and elemental composition of Fe(III)-precipitates formed in aerated Fe(II) and As(III) containing water. Geochim. Cosmochim. Acta. 74(20), 5798-5816.

Kashyap, S., Woehl, T.J., Liu, X., Mallapragada, S.K., Prozorov, T., 2014. Nucleation of iron oxide nanoparticles mediated by Mms6 protein *in situ*. ACS Nano. 8(9), 9097-9106.

Kleber, M., Eusterhues, K., Keiluweit, M., Mikutta, C., Mikutta, R., Nico, PS., 2015. Mineral-organic associations: Formation, properties, and relevance in soil environments. Adv. Agron. 130, 1-140.

Lai, Y.M., Liang, X.F., Yang, S.Y., Wang, J.X., Cao, L.H., Dai, B., 2011. Raman and FTIR spectra of iron phosphate glasses containing cerium. J. Mol. Struct. 992(1-3), 84-88.

Li, L., Stanforth, R., 2000. Distinguishing adsorption and surface precipitation of phosphate on goethite (α-FeOOH). J. Colloid Interface Sci. 230(1), 12-21.

Liu, C., Huang, P.M., 2003. Kinetics of lead adsorption by iron oxides formed under the influence of citrate. Geochim. Cosmochim. Acta. 67(5), 1045-1054.

Loeppert, R.H., Inskeep, W.P., 1996. Methods of soil analysis. Part 3, chemical methods, in Sparks et al. (ed.), Book series No 5 SSSA and ASA, Madison, pp. 639- 664.

Magid, J., Tiessen, H., Condron, L.M., 1996. Dynamics of organic phosphorus in soils under natural and agricultural ecosystems, in: Piccolo, A. (Ed), Humic substances in terrestrial ecosystems. Elsevier Science, Amsterdam, pp. 429-466.

Mallet, M., Barthélémy, K., Ruby, C., Renard, A., Naille, S., 2013. Investigation of phosphate adsorption onto ferrihydrite by X-ray Photoelectron Spectroscopy. J. Colloid Interface Sci. 407, 95-101.

Mao, Y., Pham, A.N., Rose, A.L., Waite, T.D., 2011. Influence of phosphate on the oxidation kinetics of nanomolar Fe(II) in aqueous solutions at circumneutral pH. Geochim. Cosmochim. Acta. 75(16), 4601-4610.

Martin, C.J., Evans, W.J., 1987. Phytic acid: divalent cation interactions. V. titrimetric, calorimetric, and binding studies with cobalt(II) and nickel(II) and their comparison with other metal ions. J. Inorg. Biochem. 30(2), 101-119.

Martin, M., Celi, L., Barberis, E., 1999. Determination of low concentrations of organic phosphorus in soil solution. Commun. Soil Sci. Plant Anal. 30(13-14), 1909-1917.

Mikutta, C., Mikutta, R., Bonneville, S., Wagner, F., Voegelin, A., Christl, I., Kretzschmar, R., 2008. Synthetic coprecipitates of exopolysaccharides and ferrihydrite. Part I: Characterization. Geochim. Cosmochim. Acta. 72(4), 1111-1127.

Mikutta, R., Lorenz, D., Guggenberger, G., Haumaier, L., Freund, A., 2014. Properties and reactivity of Fe-organic matter associations formed by coprecipitation *versus* adsorption: Clues from arsenate batch adsorption. Geochim. Cosmochim. Acta. 144, 258–276.

Mitra, A.K., Matthews, M.L., 1985. Effects of pH and phosphate on the oxidation of iron in aqueous solution. Int. J. Pharm. 23(2), 185-193.

Moncelli, M.R., Becucci. L., Guidelli, R., 1994. The intrinsic pKa values for phosphatidylcholine, phosphatidylethanolamine, and phosphatidylserine in monolayers deposited on mercury electrodes. Biophys. J. 66(6), 1969-1980.

Moulder, J.F., Stickle, W.F., Sobol, P.E., Bomben, K.D., 1995. Handbook of X-ray Photoelectron Spectroscopy. Chastain, J. (ed.), Perkin-Elmer Corporation, Physical Electronics Division, Minneapolis.

Ognalaga, M., Frossard, E., Thomas, F., 1994. Glucose-1-phosphate and *myo*-inositol hexaphosphate adsorption mechanisms on goethite. Soil Sci. Soc. Am. J. 58(2), 332-337.

Ohno, T., Zibilske, L.M., 1991. Determination of low concentration of phosphorus in soil extracts using malachite green. Soil Sci. Soc. Am. J. 55(3), 892-895.

Pédrot, M., Le Boudec, A., Davranche, M., Dia, A., Henin, O., 2011. How does organic matter constrain the nature, size and availability of Fe nanoparticles for biological reduction? J. Colloid Interface Sci. 359(1), 75-85.

Persson, P., Nilsson, N., Sjöberg, S., 1996. Structure and bonding of orthophosphate ions at the iron oxide-aqueous interface. J. Colloid Interface Sci. 177(1), 263-275.

Pham, A.N., Waite T.D., 2008. Oxygenation of Fe(II) in the presence of citrate in aqueous solution at pH 6.0-8.0 and 25 °C: Interpretation from an Fe(II)/citrate speciation perspective. J. Phys. Chem. A. 112(4), 643-651.

Senn, A.C., Kaegi, R., Hug, S.J., Hering, J.G., Mangold, S., Voegelin, A., 2015. Composition and structure of Fe(III)-precipitates formed by Fe(II) oxidation in water at near-neutral pH: Interdependent effects of phosphates, silicate and Ca. Geochim. Cosmochim. Acta. 162, 220-246.

Shimizu, M., Zhou, J., Schröder, C., Obst, M., Kappler, A., Borch, T., 2013. Dissimilatory reduction and transformation of ferrihydrite-humic acid coprecipitates. Environ. Sci. Technol. 47(23), 13375-13384.

Sodano, M., Said-Pullicino, D., Fiori, A.F., Catoni, M., Martin, M., Celi, L., 2016. Sorption of paddy soil-derived dissolved organic matter on hydrous iron oxide–vermiculite mineral phases. Geoderma. 261, 169-177.

Sodano, M., Lerda, C., Nisticò, R., Martin, M., Magnacca, G., Celi, L., Said-Pullicino, D., 2017. Dissolved organic carbon retention by coprecipitation during the oxidation of ferrous iron. Geoderma. 307, 19-29.

Thibault, P.J., Rancourt, D.G., Evans, R.J., Dutrizac, J.E., 2009. Mineralogical confirmation of a near-P:Fe = 1:2 limiting stoichiometric ratio in colloidal P-bearing ferrihydrite-like hydrous ferric oxide. Geochim. Cosmochim. Acta. 73(2), 364‑376.

van der Grift, B., Behrends, T., Osté, L.A., Schot, P.P., Wassen, M.J., Griffioen, J., 2016. Fe hydroxyphosphate precipitation and Fe(II) oxidation kinetics upon aeration of Fe(II) and phosphate-containing synthetic and natural solution. Geochim. Cosmochim. Acta. 186, 71-90.

Voegelin, A., Kaegi, R., Frommer, J., Vantelon, D., Hug, S.J., 2010. Effect of phosphate, silicate, and Ca on Fe(III)-precipitates formed in aerated Fe(II)- and As(III)-containing water studied by X-ray absorption spectroscopy. Geochim. Cosmochim. Acta. 74(1), 164-186.

Voegelin, A., Senn, A.C., Kaegi, R., Hug, S.J., Mangold, S., 2013. Dynamic Fe-precipitate formation induced by Fe(II) oxidation in aerated phosphate-containing water. Geochim. Cosmochim. Acta. 117, 216-231.

Wan, B., Yan, Y., Liu, F., Tan, W., He, J., Feng, X., 2016. Surface speciation of *myo*-inositol hexakisphosphate adsorbed on TiO_2 nanoparticles and its impact on their colloidal stability in aqueous suspension: A comparative study with orthophosphate. Sci. Total Environ. 544,0134-142.

Xu, J., Stevens, M.J., Oleson, T.A., Last, J.A., Sahai, N., 2009. Role of oxide surface chemistry and phospholipid phase on adsorption and self-assembly: Isotherms and atomic force microscopy. J. Phys. Chem. C. 113(6), 2187-2196.

Yan, Y., Li, W., Yang, J., Zheng, A., Liu, F., Feng, X., Sparks, D.L., 2014. Mechanism of *myo*-inositol hexakisphosphate sorption on amorphous aluminum hydroxide: Spectroscopic evidence for rapid surface precipitation. Environ. Sci. Technol. 48(12), 6735-6742.

Yang, Z., Zhang, C., Sun, Y., Ren, X., 2012. Controlled growth of calcium phosphate using phosphatidylcholine-modified porous titania as reaction compartments. Chem. Eng. Sci. 79, 112-118.

Yanyu, X., Yunmei, S., Zhipeng, C., Qineng, P., 2006. The preparation of silybin-phospholipid complex and the study on its pharmacokinetics in rats. Int. J. Pharm. 307(1), 77-82.

Zhang, Y.S., Werner, W., Scherer, H.W., Sun, X., 1994. Effect of organic manure on organic phosphorus fractions in two paddy soils. Biol. Fertil. Soils. 17(1), 64-68.

Figure captions

Fig. 1: P retention by adsorption (empty symbols) and coprecipitation (full symbols) of (a) inorganic phosphate (Pi), (b) *myo*-inositol hexaphosphate (*myo*InsP6), (c) phosphatidylcholine (PC) with increasing initial molar $(P/Fe)_0$ ratios.

Fig. 2: Variations in the amount of precipitated total Fe (a) and H^+ released (b) relative to the initial amount (Fe_0) as a function of time during the oxidative preparation of Fh. The points represent mean of three replicates (standard error always lower than 5%).

Fig. 3: Variations in the amount of precipitated total Fe (a, d, g), P retained (b, e, h) and H^+ released (c, f, i) as a function of time during the oxidative preparation of inorganic phosphate (a, b, c), *myo*-inositol hexaphosphate (d, e, f) and phosphatidylcholine (g, h, i) coprecipitates with increasing initial molar $(P/Fe)_0$ ratios. The points represent mean of three replicates (standard error always lower than 5%). Different symbols represent different initial molar $(P/Fe)_0$ ratios. Pi, inorganic phosphate; *myo*InsP6, *myo*-inositol hexaphosphate; PC, phosphatidylcholine.

Fig. 4: X-ray diffractograms of adsorbed and coprecipitated systems. Series labels represent different initial molar $(P/Fe)_0$ ratios. Pi, inorganic phosphate; *myo*InsP6, *myo*-inositol hexaphosphate; PC, phosphatidylcholine.

Fig. 5: FT-IR spectra of adsorbed and coprecipitated systems in the 1400-400 cm^{-1} region. Series labels represent different initial molar $(P/Fe)_0$ ratios. Pi, inorganic phosphate; *myo*InsP6, *myo*-inositol hexaphosphate; PC, phosphatidylcholine.

Fig. 6: XPS spectra (Fe peaks) of adsorbed and coprecipitated systems. Series labels represent different initial molar $(P/Fe)_0$ ratios. Pi, inorganic phosphate; *myo*InsP6, *myo*-inositol hexaphosphate; PC, phosphatidylcholine.

Fig. 7: XPS spectra (P peaks) of inorganic phosphate (Pi) coprecipitated systems. Series labels represent different initial molar $(P/Fe)_0$ ratios.

Fig. 8 Bright field TEM images of Fh and of lowest and highest $(P/Fe)_0$ coprecipitation products. Pi, inorganic phosphate; *myo*InsP6, *myo*-inositol hexaphosphate; PC, phosphatidylcholine.

Tables

Table 1
Langmuir and Henry coefficients of adsorption isotherms of $H_2PO_4^-$ (Pi), *myo*-inositol hexaphosphate (*myo*InsP6) and phosphatidylcholine (PC) on ferrihydrite.

P form	Isotherm	Coefficients
Pi	Langmuir $Q_a = \frac{Q_{max} \cdot C_e \cdot K_L}{1 + K_L \cdot C_e}$	$Q_{max} = 1.34$ µmol m^{-2} $K_L = 89.3$ L mmol^{-1} $R^2 = 0.817$
*myo*InsP6	Langmuir	$Q_{max} = 2.59$ µmol m^{-2} $K_L = 67.3$ L mmol^{-1} $R^2 = 0.805$
PC	Henry $Q_a = K \cdot C_e + m$	$m = 0.54$ µmol m^{-2} $K = 78.2$ ml m^{-2} $R^2 = 0.880$

Table 2
Specific surface area (SSA), total mesopore volume, ζ potential and element composition of the coprecipitated and adsorbed systems.

Sample	SSA (m^2 g^{-1})	Mesopore volume (mm^3 g^{-1})	ζ potential (mV)	Chemical P/Fe ratio	XPS P/Fe ratio
Fh	385	360	28	-	-
COP 0.05 Pi	333	451	23	0.05	0.14
COP 0.1 Pi	317	446	12	0.11	0.23
COP 0.5 Pi	194	850	2	0.47	1.15
COP 1 Pi	176	1200	−11	0.78	1.53
ADS 0.05 Pi	327	453	22	0.05	0.13
ADS 0.1 Pi	323	490	16	0.05	0.16
ADS 0.5 Pi	307	486	10	0.08	0.25
ADS 1 Pi	293	564	−18	0.17	0.22
COP 0.05 *myo*InsP6	279	448	20	0.05	0.05
COP 0.1 *myo*InsP6	264	516	8	0.11	0.20
COP 0.5 *myo*InsP6	193	882	−38	0.48	0.92
COP 1 *myo*InsP6	191	859	−47	1.01	1.79
ADS 0.05 *myo*InsP6	275	465	−14	0.04	0.13
ADS 0.1 *myo*InsP6	294	397	−38	0.16	0.18
ADS 0.5 *myo*InsP6	301	433	−44	0.33	0.34
ADS 1 *myo*InsP6	272	593	−62	0.24	0.35
COP 0.025 PC	145	250	12	0.04	0.09
COP 0.05 PC	~31	65	34	0.05	0.11
COP 0.1 PC	~2	36	22	0.11	1.47
COP 0.5 PC	~5	1	7	0.44	9.18
ADS 0.025 PC	145	266	16	0.05	0.09
ADS 0.05 PC	~64	139	33	0.05	0.08
ADS 0.1 PC	~2	7	21	0.07	0.49
ADS 0.5 PC	~4	11	7	0.31	2.90

Table 3

Dissociation acid constants of phosphoric acid (Corbridge, 1985), *myo*-inositol hexakisphosphoric acid (Costello et al., 1976) and phosphatidylcholine (Moncelli et al., 1994).

Molecule	pK_1	$pK_{2,3}$	$pK_{4,6}$	pK_7	pK_8	pK_9	$pK_{10,11}$	pK_{12}
phosphoric acid	2.0	6.8	12.3					
myo-inositol hexakisphosphoric acid	1.1	1.5	1.8	5.7	6.9	7.6	10.0	12.0
phosphatidylcholine	0.8							

Figures

Fig. 1

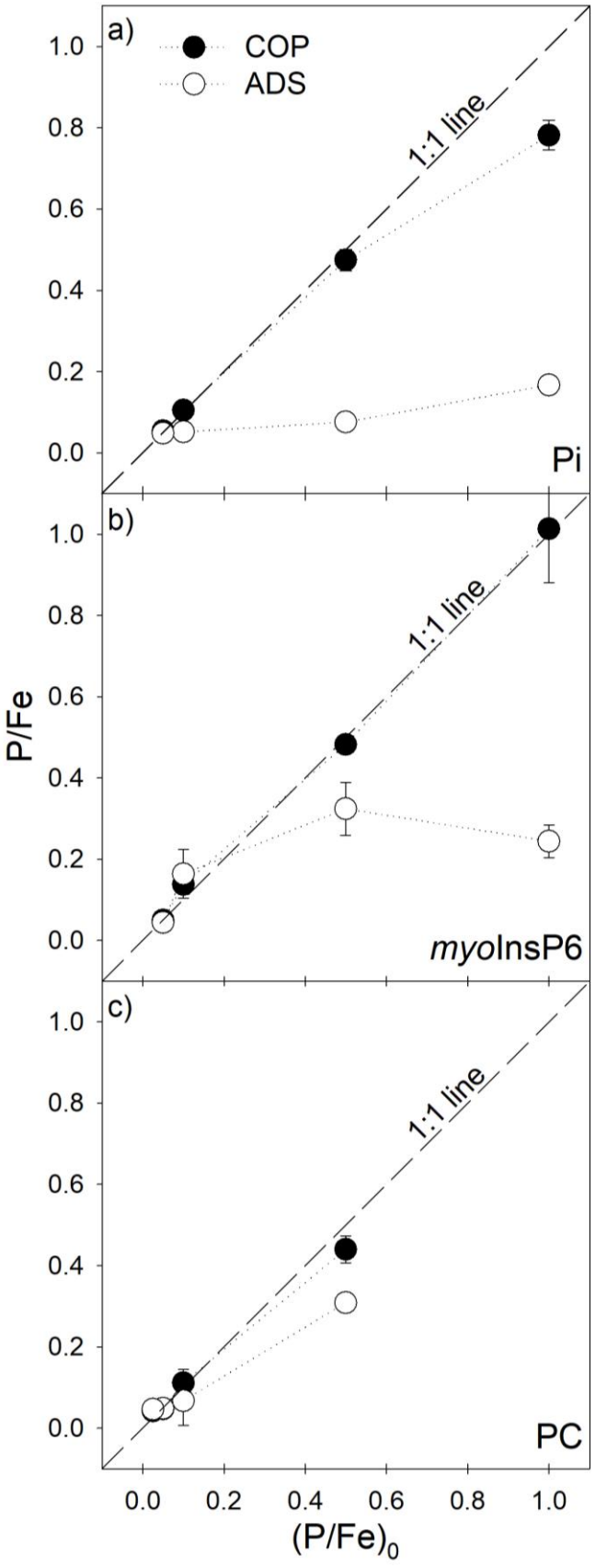

Fig. 2

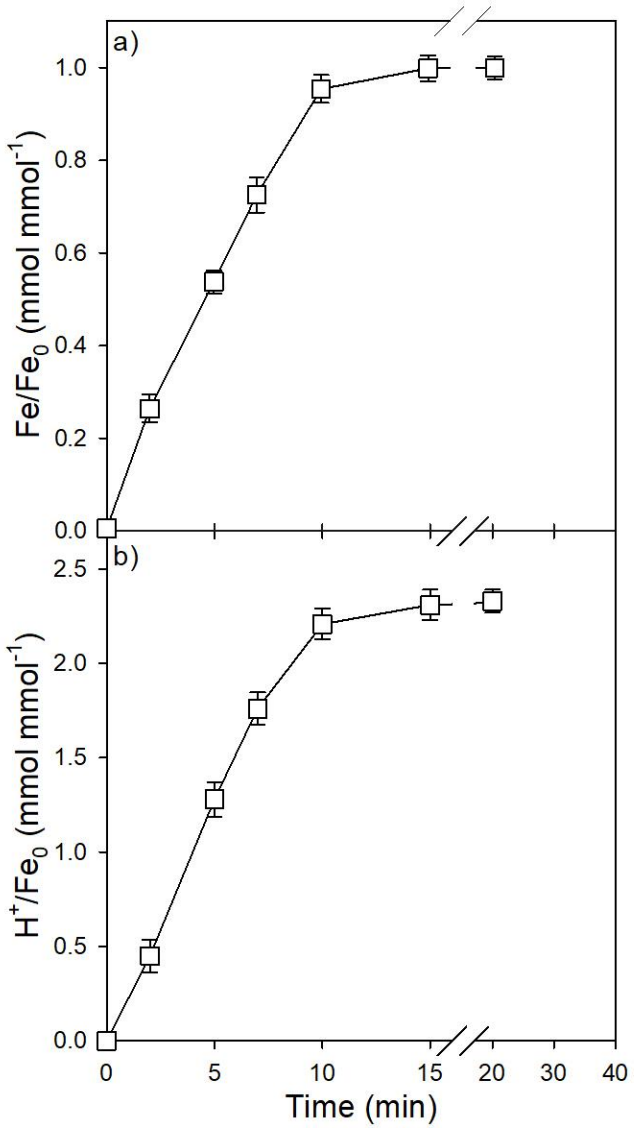
a)
b)
Fe/Fe0 (mmol mmol-1)
H+/Fe0 (mmol mmol-1)
Time (min)
0.0
0.2
0.4
0.6
0.8
1.0
0.5
1.5
2.0
2.5
0
5
10
15
20
30
40

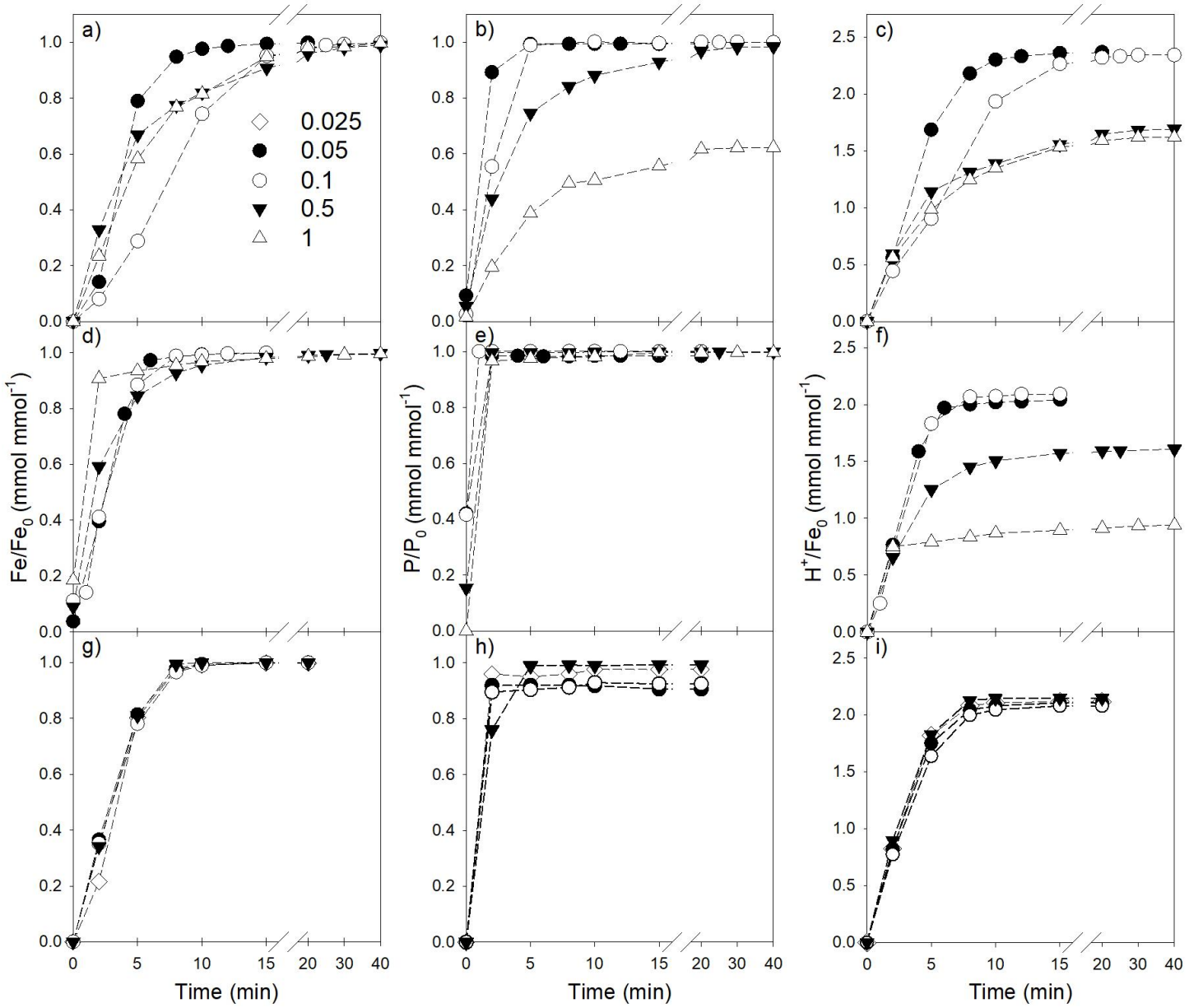
a)
b)
c)
d)
e)
f)
g)
h)
i)
0.025
0.05
0.1
0.5
1
Fe/Fe0 (mmol mmol-1)
P/P0 (mmol mmol-1)
H+/Fe0 (mmol mmol-1)
Time (min)
Time (min)
Time (min)

Fig. 3

Fig. 4

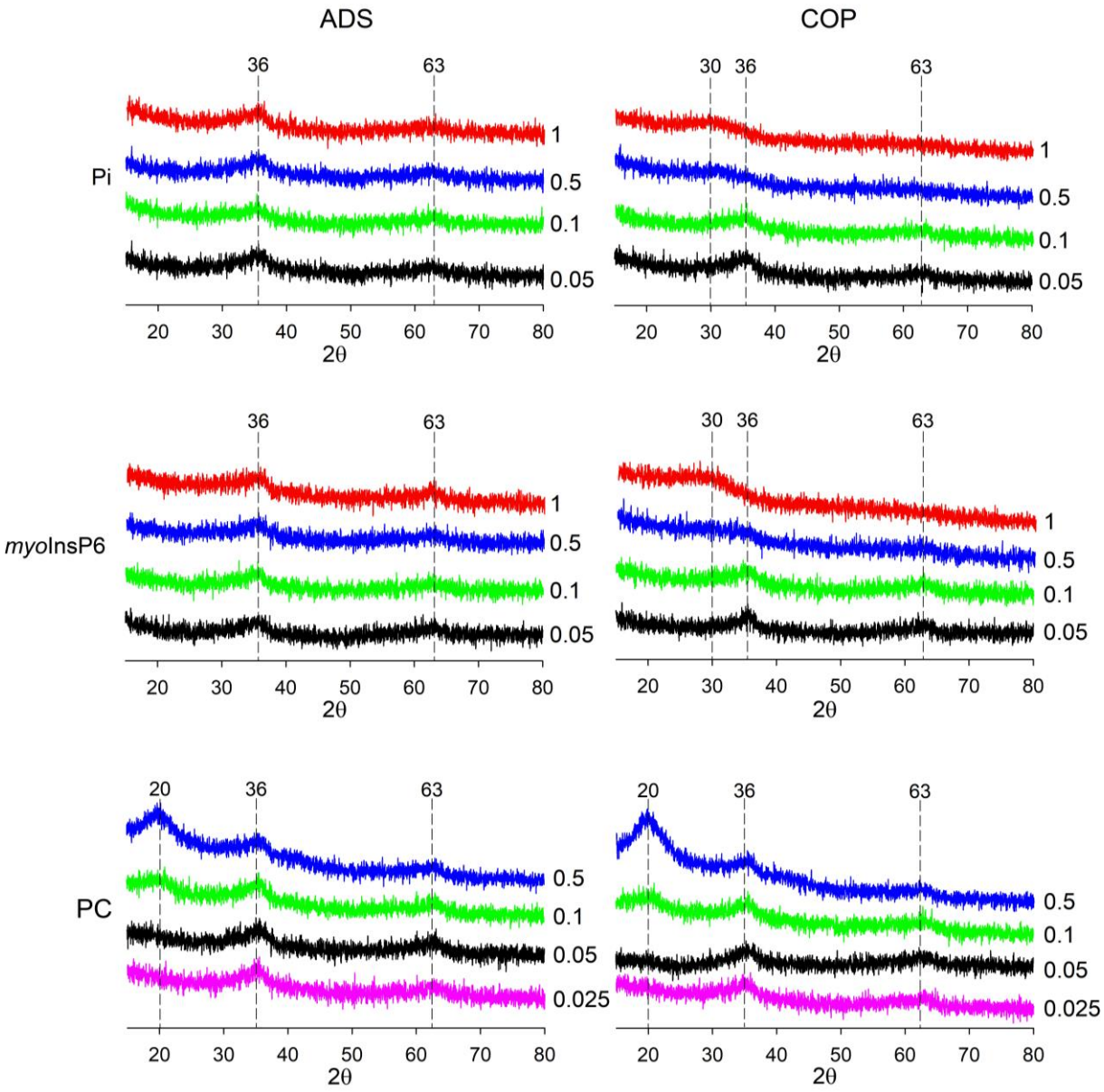
ADS
COP
Pi
myoInsP6
PC
36
63
30
20
1
0.5
0.1
0.05
0.025
20 30 40 50 60 70 80
2θ

Fig. 5

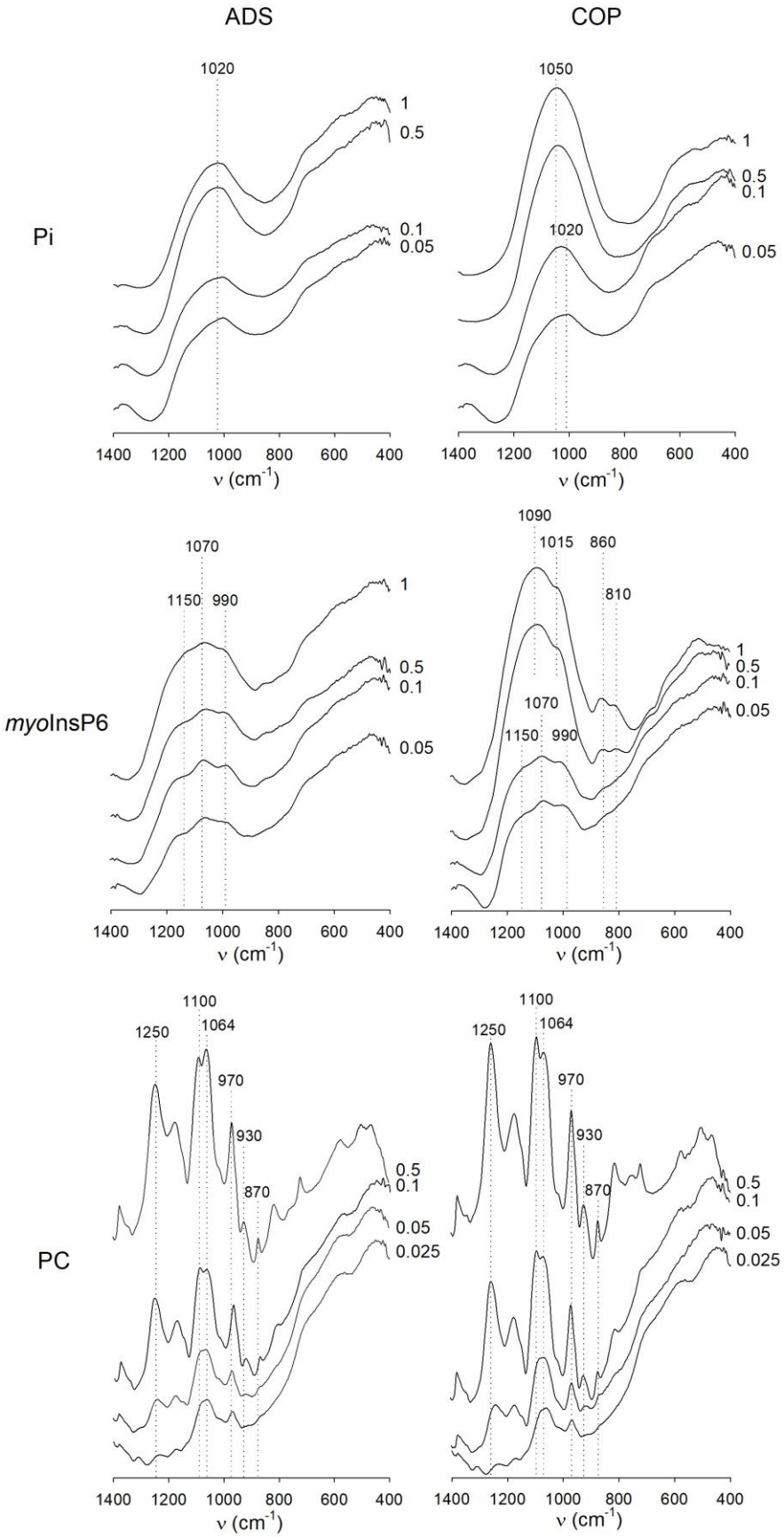
ADS
COP
Pi
1020
1050
1
0.5
0.1
0.05
0.025
1400 1200 1000 800 600 400
ν (cm-1)
myoInsP6
1070
1150 990
1090
1015 860
810
PC
1100
1064
1250
970
930
870

Fig. 6

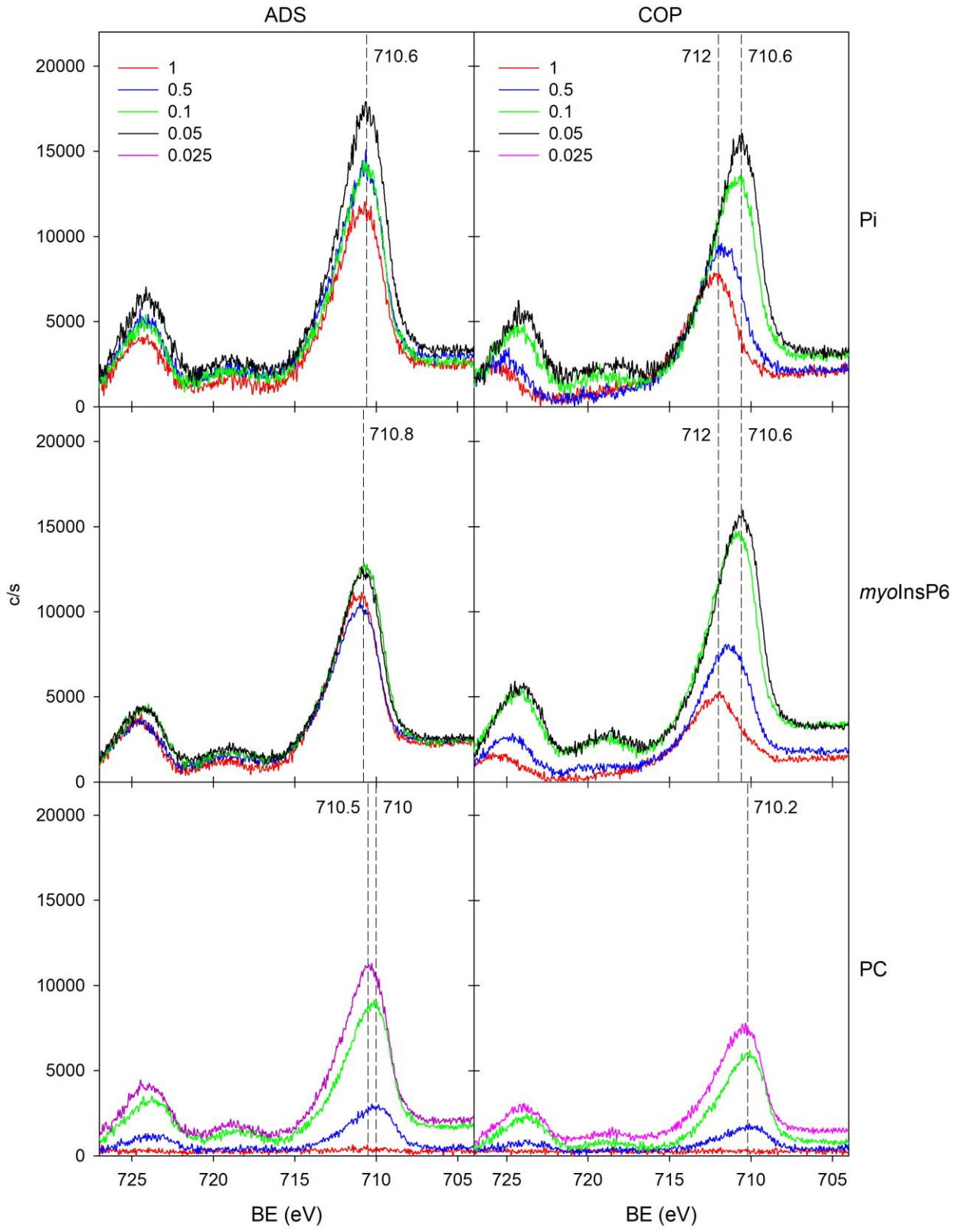
ADS
COP
1
0.5
0.1
0.05
0.025
710.6
712
710.6
710.8
712
710.6
710.5
710
710.2
Pi
myoInsP6
PC
c/s
BE (eV)
BE (eV)
20000
15000
10000
5000
0
725
720
715
710
705

Fig. 7

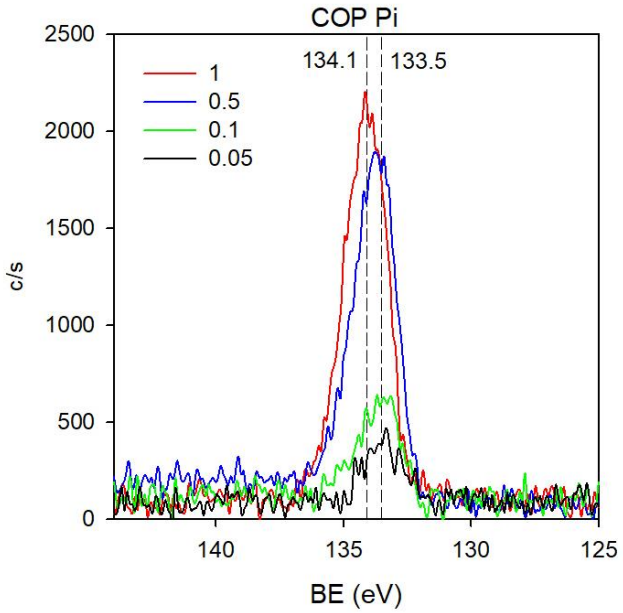
COP Pi
134.1
133.5
1
0.5
0.1
0.05
c/s
2500
2000
1500
1000
500
0
140
135
130
125
BE (eV)

Fig. 8

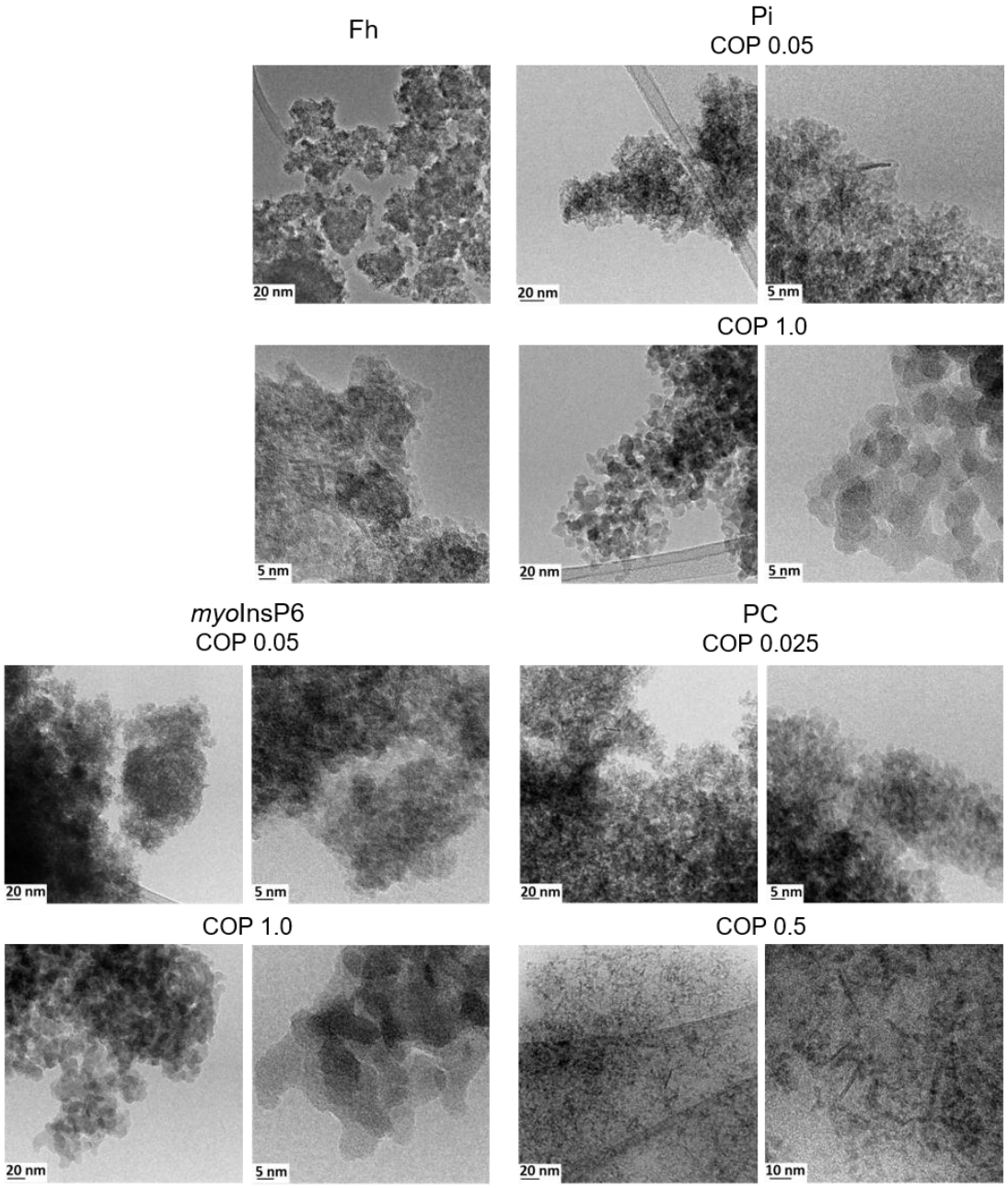
Fh
Pi
COP 0.05
20 nm
20 nm
5 nm
COP 1.0
5 nm
20 nm
5 nm
*myo*InsP6
COP 0.05
PC
COP 0.025
20 nm
5 nm
20 nm
5 nm
COP 1.0
COP 0.5
20 nm
5 nm
20 nm
10 nm